JOURNAL OF COMPUTATIONAL PHYSICS **138,** 57–82 (1997)
ARTICLE NO. CP975815

Finite Difference Methods for 3D Viscous Incompressible Flows in the Vorticity–Vector Potential Formulation on Nonstaggered Grids

Weinan E* and Jian-Guo Liu†

*Courant Institute of Mathematical Sciences, New York, New York 08540; †Department of Mathematics, Temple University, Philadelphia, Pennsylvania 19122
E-mail: weinan@cims.nyu.edu; jliu@math.temple.edu

Received May 16, 1996; revised July 31, 1997

Simple, efficient, and accurate finite difference methods are introduced for 3D unsteady viscous incompressible flows in the vorticity–vector potential formulation on nonstaggered grids. Two different types of methods are discussed. They differ in the implementation of the normal component of the vorticity boundary condition and consequently the enforcement of the divergence free condition for vorticity. Both second-order and fourth-order accurate schemes are developed. A detailed accuracy test is performed, revealing the structure of the error and the effect of how the convective terms are discretized near the boundary. The influence of the divergence free condition for vorticity to the overall accuracy is studied. Results on the cubic driven cavity flow at Reynolds number 500 and 3200 are shown and compared with that of the MAC scheme. © 1997 Academic Press

1. INTRODUCTION

The purpose of this paper is to present efficient, stable, and accurate finite difference schemes in the vorticity–vector potential formulation for computing the dynamics of viscous incompressible fluids. *The emphasis is on three dimensions and nonstaggered grids*. Very efficient and stable second- and fourth-order accurate difference schemes based on vorticity–stream function formulation already exist in two dimensions [2, 3]. It is well known that there is a major difference between two and three dimensions for vorticity-based numerical methods. Most apparent of all is the fact that both vorticity and stream function become vector (instead of scalar) fields in 3D. At the same time, stream function changes its name to vector

0021-9991/97 $25.00
Copyright © 1997 by Academic Press
All rights of reproduction in any form reserved.

potential. Along with this is the necessity to enforce divergence free conditions for vorticity and vector potential. This turns out to be a major problem in designing efficient numerical methods in 3D based on this formulation.

One way of overcoming these difficulties is to use a staggered grid [6, 8, 14, 10]. Ever since the pioneering work of Harlow and Welch on MAC scheme [5], staggered grid has been a very effective tool in dealing with the numerical difficulties in discretizing the *div*, *curl*, and *grad* operators. This is no exception for the 3D vorticity-based finite difference methods. Indeed much work has been done on staggered grids, mainly with the vorticity–velocity formulation [6, 8, 14, 10]. Nevertheless, because the variables are defined on the surfaces of two sets of mutually dual grids (hence six different grids are involved), extending to nonrectangular grids becomes prohibitively expensive and has never been done. In addition, since the variables are not defined at the same grid point, accurately evaluating the nonlinear convective terms becomes an issue.

In this paper, we introduce a second-order accurate method based on the vorticity–vector potential formulation on the nonstaggered grid whose performance on uniform grids is comparable with the MAC scheme. This appears to be the first such method on nonstaggered grids. We will pay special attention to how accurately the divergence-free conditions for vorticity, velocity, and vector potential are satisfied. We will derive the three-dimensional analog of the local vorticity boundary conditions such as Thom's formula. Detailed accuracy checks on smooth solutions reveals a distinct structure for the error (see Fig. 1). Consequently straightforward discretization of the convective terms using the vorticity boundary condition can lead to a loss of accuracy near the boundary. In addition, when applied to the standard test problem—the cubic driven cavity flow, most discretization techniques for the convective terms results in a scheme that is susceptible to Gibbs-like phenomena at the edges where the flow becomes singular. This in turn makes the method essentially useless for high Reynolds number flows. We present a simple way of circumventing this problem and compare results of our method with that of the MAC scheme for both low (Re = 500) and high (Re = 3200) Reynolds number flows.

From a numerical point of view we follow the same philosophy as advocated in [2, 3], namely that we will insist on discretizing the viscous term explicitly and using local vorticity boundary conditions. Consequently this method is not intended for use at very low Reynolds numbers for which the flow converges to a steady state. However, as long as there is nontrivial dynamics, this method will be a very attractive alternative to the projection method.

This paper is organized as follows. In Section 2, we will present some formulations of the Navier–Stokes equations (both new and old) in vorticity variable and the basic second-order finite difference methods that we will work with. Results of a detailed accuracy test will be presented in Section 3. The error in the vorticity-based methods has a special structure (see Fig. 1) associated with the vorticity boundary conditions, and this has important implications on how the convective terms should be discretized near the boundary. In Section 4 we will study the cubic driven cavity flows at Reynolds numbers 500 and 3200. In particular we will look at the influence of the singular behavior at the upper edges of the cavity. In Section 5 we will study the issue of divergence-free condition for vorticity by examining a

slightly different method which enforces this condition indirectly. In Section 6 we summarize the important aspects of the method put forward in this paper. Finally in the appendices we present extensions to fourth-order accuracy as well as in- and out-flow boundary conditions.

Before ending this introduction, let us mention that the interest in designing numerical methods using the vorticity formulation goes beyond hydrodynamics. It has an effect on understanding in general how to discretize the *div*, *curl*, and *grad* operators. This is useful for a broad spectrum of problems including electromagnetism, micro-magnetics, superconductivity, and magnetohydrodynamics.

Some of the results in this paper were announced in [4].

2. FORMULATIONS OF THE NAVIER–STOKES EQUATION AND THE DIFFERENCE METHODS

Our starting point is the incompressible Navier–Stokes equation in the vorticity form:

$$\begin{aligned} &\frac{\partial \boldsymbol{\omega}}{\partial t} + \nabla \times (\boldsymbol{\omega} \times \boldsymbol{u}) = \nu \Delta \boldsymbol{\omega}, \\ &\boldsymbol{\omega} = \nabla \times \boldsymbol{u}, \quad \nabla \cdot \boldsymbol{u} = 0, \\ &\boldsymbol{u}(\boldsymbol{x}, 0) = \boldsymbol{u}_0(\boldsymbol{x}). \\ &\boldsymbol{u} = \boldsymbol{u}_b \quad \text{at the boundary.} \end{aligned} \tag{2.1}$$

where $\boldsymbol{u}$ is the velocity and $\boldsymbol{\omega}$ is the vorticity. Since $\boldsymbol{u}$ is divergence-free, we can introduce the analog of stream function in 2D:

$$\boldsymbol{u} = \nabla \times \boldsymbol{\psi}. \tag{2.2}$$

In accordance with electromagnetism, $\boldsymbol{\psi}$ is usually referred to as the vector potential. Unlike stream function in 2D, vector potential in 3D is far from being uniquely defined: If $\boldsymbol{\psi}$ satisfies (2.2) and ξ is a smooth scalar function, then $\boldsymbol{\psi} + \nabla\xi$ also satisfies (2.2). This is the gauge freedom. To fix the gauge, consider

$$\boldsymbol{\omega} = \nabla \times (\nabla \times \boldsymbol{\psi}) = \nabla(\nabla \cdot \boldsymbol{\psi}) - \Delta \boldsymbol{\psi}. \tag{2.3}$$

If we want to maintain a Poisson equation between $\boldsymbol{\psi}$ and $\boldsymbol{\omega}$, we need to enforce

$$\nabla \cdot \boldsymbol{\psi} = 0. \tag{2.4}$$

Note that for some formulations it is enough to have

$$\nabla \cdot \boldsymbol{\psi}|_{\partial\Omega} = 0 \tag{2.5}$$

in order to ensure (2.4).

The three divergence-free conditions,

$$\nabla \cdot \boldsymbol{\omega} = 0, \quad \nabla \cdot \boldsymbol{u} = 0, \quad \nabla \cdot \boldsymbol{\psi} = 0, \tag{2.6}$$

are the main new difficulties for numerical methods based on the vorticity formulation in 3D. Among these three conditions, the second is usually trivially satisfied by letting $\boldsymbol{u} = \nabla \times \boldsymbol{\psi}$. The third is very much a consequence of the first, and the first is the most difficult to enforce. In this paper we will develop two methods and their only difference is in the enforcement of the divergence-free condition for vorticity. In this way we can study the influence of the accuracy of the divergence-free conditions on the overall accuracy of the methods.

2.1. *The $\boldsymbol{\omega}$-$\boldsymbol{\psi}$ Formulation*

We will consider the case when $\boldsymbol{u}_b \cdot \boldsymbol{n} = 0$ (where $\boldsymbol{n}$ is the outward normal at the boundary), i.e. no in-flow and out-flow. The modifications needed at in-flow and out-flow boundaries will be given in the Appendix.

PROPOSITION 1. *Equations* (2.1)–(2.2) *are equivalent to*

$$\begin{aligned} &\frac{\partial \boldsymbol{\omega}}{\partial t} + \nabla \times [\boldsymbol{\omega} \times (\nabla \times \boldsymbol{\psi})] = \nu \Delta \boldsymbol{\omega}, \\ &-\Delta \boldsymbol{\psi} = \boldsymbol{\omega}, \end{aligned} \tag{2.7}$$

with boundary conditions

$$\begin{aligned} &\boldsymbol{n} \times \boldsymbol{\psi} = 0, \quad \frac{\partial}{\partial \boldsymbol{n}} (\boldsymbol{\psi} \cdot \boldsymbol{n}) = 0 \quad \text{on } \Gamma = \partial\Omega \\ &\boldsymbol{n} \cdot \boldsymbol{\omega} = \boldsymbol{n} \cdot \nabla \times \boldsymbol{u}, \quad \boldsymbol{n} \times \boldsymbol{u}_b = \boldsymbol{n} \times \nabla \times \boldsymbol{\psi} \quad \text{on } \Gamma = \partial\Omega \end{aligned} \tag{2.8}$$

and initial condition

$$\boldsymbol{\omega}_0(\boldsymbol{x}) = \nabla \times \boldsymbol{u}_0(\boldsymbol{x}). \tag{2.9}$$

Proof. For simplicity of presentation we will only consider the case when Ω = upper half space and $\partial\Omega$ = xy-plane.

Let $(\boldsymbol{\omega}, \boldsymbol{u})$ be a smooth solution of (2.1). We want to show that it gives rise to a solution of (2.7)–(2.9). Define $\boldsymbol{\psi}$ by

$$\begin{aligned} &-\Delta \boldsymbol{\psi} = \boldsymbol{\omega} \quad \text{on } \Omega \\ &\psi_1 = \psi_2 = 0, \quad \frac{\partial \psi_3}{\partial z} = 0 \quad \text{on } \Gamma. \end{aligned} \tag{2.10}$$

The boundary condition of $\boldsymbol{\psi}$ in (2.10) implies that

$$\nabla \cdot \boldsymbol{\psi} = 0 \quad \text{on } \Gamma.$$

Being a solution of (2.1), $\boldsymbol{\omega}$ must satisfy

$$\nabla \cdot \boldsymbol{\omega} = 0 \quad \text{on } \Omega.$$

Therefore we have

$$\begin{aligned} -\Delta(\nabla \cdot \boldsymbol{\psi}) &= 0 \quad \text{on } \Omega \\ \nabla \cdot \boldsymbol{\psi} &= 0 \quad \text{on } \Gamma. \end{aligned} \tag{2.11}$$

Hence,

$$\nabla \cdot \boldsymbol{\psi} = 0 \quad \text{on } \Omega.$$

Now we can rewrite the first equation in (2.10) as

$$\nabla \times (\boldsymbol{u} - \nabla \times \boldsymbol{\psi}) = 0.$$

Since

$$\nabla \cdot (\boldsymbol{u} - \nabla \times \boldsymbol{\psi}) = 0$$

and

$$(\boldsymbol{u} - \nabla \times \boldsymbol{\psi}) \cdot \boldsymbol{n} = 0 \quad \text{on } \Gamma,$$

where $\boldsymbol{n} = (0, 0, 1)$, we get

$$\boldsymbol{u} = \nabla \times \boldsymbol{\psi}$$

on Ω, and on $\overline{\Omega}$ by continuity. This shows that $(\boldsymbol{\omega}, \boldsymbol{\psi})$ solves (2.7)–(2.9). Here we have made use of the fact that on a simply-connected domain, if a vector field $\boldsymbol{v}$ satisfies $\nabla \times \boldsymbol{v} = 0$, $\nabla \cdot \boldsymbol{v} = 0$, and the boundary condition $\boldsymbol{v} \cdot \boldsymbol{n} = 0$, then $\boldsymbol{v} = 0$. A simple proof of this fact is the following. From the first condition, we can write $\boldsymbol{v}$ as $\boldsymbol{v} = \nabla \phi$ for some scalar field ϕ. The second condition gives $\Delta \phi = 0$. This, together with the boundary condition $\partial \phi / \partial \boldsymbol{n} = 0$ implies $\phi = \text{const}$. Hence $\boldsymbol{v} = 0$.

Conversely let $(\boldsymbol{\omega}, \boldsymbol{\psi})$ be a solution of (2.7)–(2.9). We first take a look at the initial condition $(\boldsymbol{\omega}_0, \boldsymbol{u}_0, \boldsymbol{\psi}_0)$. Given $\boldsymbol{u}_0$, $\boldsymbol{\omega}_0$ is given from (2.9), and $\boldsymbol{\psi}_0$ from (2.10). The previous argument implies that

$$\nabla \cdot \boldsymbol{\psi}_0 = 0, \quad \boldsymbol{u}_0 = \nabla \times \boldsymbol{\psi}_0.$$

Taking divergence on both sides of the first equation in (2.6), we get

$$\frac{\partial}{\partial t} [\Delta(\nabla \cdot \boldsymbol{\psi})] = \nu [\Delta^2 (\nabla \cdot \boldsymbol{\psi})] \quad \text{on } \Omega.$$

From (2.8), we have

$$\partial_x^2 \psi_3 = \partial_x \partial_z \psi_1 - \partial_x u_{2b}, \quad \partial_y^2 \psi_3 = \partial_y \partial_z \psi_2 + \partial_y u_{1b} \quad \text{on } \Gamma. \tag{2.12}$$

Since

$$\omega_3 = -(\partial_x^2 \psi_3 + \partial_y^2 \psi_3 + \partial_z^2 \psi_3),$$

using (2.12) we have

$$\frac{\partial(\nabla \cdot \boldsymbol{\psi})}{\partial \boldsymbol{n}} = \partial_z(\partial_x \psi_1 + \partial_y \psi_2 + \partial_z \psi_3) = -\omega_3 + \partial_x u_{2b} - \partial_y u_{1b} = 0 \quad \text{on } \Gamma.$$

Therefore $\nabla \cdot \boldsymbol{\psi}$ satisfies the system of equations

$$\begin{aligned} \frac{\partial}{\partial t}[\Delta(\nabla \cdot \boldsymbol{\psi})] &= \nu[\Delta^2(\nabla \cdot \boldsymbol{\psi})] \quad \text{on } \Omega, \\ (\nabla \cdot \boldsymbol{\psi})|_\Gamma &= 0, \\ \frac{\partial(\nabla \cdot \boldsymbol{\psi})}{\partial \boldsymbol{n}} &= 0 \quad \text{on } \Gamma. \end{aligned}$$

Since at $t = 0$, $\nabla \cdot \boldsymbol{\psi} = 0$, we get

$$\nabla \cdot \boldsymbol{\psi} = 0 \quad \text{on } \Omega$$

for all time. This is a consequence of the uniqueness of solutions to the above problem. Therefore if we define $\boldsymbol{u} = \nabla \times \boldsymbol{\psi}$, we have

$$\nabla \times \boldsymbol{u} = \nabla \times (\nabla \times \boldsymbol{\psi}) = -\Delta \boldsymbol{\psi}.$$

Clearly $\boldsymbol{u}$ also satisfies all the boundary and initial conditions in (2.1)–(2.2). This shows that $(\boldsymbol{\omega}, \boldsymbol{u})$ is a solution of (2.1)–(2.2). The proposition is proved.

Remark. The formulation (2.7)–(2.9) simplifies in the case when the boundary of the domain consists of flat surfaces parallel to the coordinate planes. The three components of the vector potential decouple, and the first set of boundary conditions in (2.8) becomes homogeneous Dirichlet boundary conditions for the tangential components of the vector potential and the Neumann boundary condition for the normal component.

This formulation of the incompressible fluid equations appears to be new. There is a very closely related formulation that already exists in the literature. For the sake of completeness we include the statement of this formulation here as our second proposition. Its proof can be found in [12].

PROPOSITION 2. *Equations* (2.1)–(2.2) *are equivalent to* (2.7) *and* (2.9) *together with the boundary conditions*

$$\begin{aligned} \boldsymbol{n} \times \boldsymbol{\psi} = 0, \quad \nabla \cdot \boldsymbol{\psi} = 0 \quad \text{on } \Gamma = \partial\Omega \\ \nabla \cdot \boldsymbol{\omega} = 0, \quad \boldsymbol{n} \times \boldsymbol{u}_b = \boldsymbol{n} \times \nabla \times \boldsymbol{\psi} \quad \text{on } \Gamma = \partial\Omega. \end{aligned} \tag{2.13}$$

As we can see, the only difference between the two formulations is in the boundary condition for the normal component of the vorticity. In Proposition 2, the Dirichlet boundary condition in Proposition 1 is replaced by the divergence-free condition which amounts to a Neumann-type boundary condition. This has the effect of imposing $\nabla \cdot \boldsymbol{\omega} = 0$ more directly. As we will see later, this has a drastic consequence on how well this condition is met numerically.

2.2. *Second-Order Finite Difference Schemes Based on the $\boldsymbol{\omega}$-$\boldsymbol{\psi}$ Formulation*

As before we will limit the discussion to the case when Ω is the upper half space. Extension to more general situations is immediate.

The basic strategy is to couple the first set of boundary conditions in (2.8) to the Poisson equations for $\boldsymbol{\psi}$ and use the second set of boundary conditions as vorticity boundary conditions for the vorticity transport equation. In particular, we will derive from them the analog of Thom's formula in 3D [13].

The numerical grid is defined by $\Omega_h = \{(x_i, y_j, z_k),\ x_i = i\ \Delta x,\ y_j = j\ \Delta y,\ z_k = k\ \Delta z,\ i, j \in Z,\ k \in Z^+\}$. For boundary conditions, we need to define the "ghost" points: $\{(x_i, y_j, z_{-1}),\ i, j \in Z,\ z_{-1} = -\Delta z\}$. We will use the difference operators:

$$\tilde{D}_x g(x, y, z) = \frac{g(x + \Delta x, y, z) - g(x - \Delta x, y, z)}{2\ \Delta x}$$

$$D_x^2 g(x, y, z) = \frac{g(x + \Delta x, y, z) - 2g(x, y, z) + g(x - \Delta x, y, z)}{\Delta x^2};$$

similarly for $\tilde{D}_y g$, $D_y^2 g$, etc.

We first describe the semi-discrete version of the method. In the interior of Ω_h (i.e., $k > 0$), we use

$$\begin{aligned} &\frac{\partial \boldsymbol{\omega}}{\partial t} + \tilde{\nabla}_h \times [\boldsymbol{\omega} \times (\nabla \times \boldsymbol{\psi})] = \nu\, \Delta_h \boldsymbol{\omega}, \\ &-\Delta_h \boldsymbol{\psi} = \boldsymbol{\omega}, \\ &\boldsymbol{u} = \tilde{\nabla}_h \times \boldsymbol{\psi}. \end{aligned} \tag{2.14}$$

The difference operators appeared here defined by

$$\Delta_h = D_x^2 + D_y^2 + D_z^2, \quad \tilde{\nabla}_h = (\tilde{D}_x, \tilde{D}_y, \tilde{D}_z).$$

The first set of boundary conditions, to be supplemented to the Poisson equations for $\boldsymbol{\psi}$, is

$$\psi_1(x_i, y_j, 0) = \psi_2(x_i, y_j, 0) = 0, \quad \frac{\psi_3(x_i, y_j, z_1) - \psi_3(x_i, y_j, z_{-1})}{2\ \Delta z} = 0 \tag{2.15}$$

for $i, j, \in Z$. Given $\{\boldsymbol{\omega}(x_i, y_j, z_k),\ i, j \in Z,\ k \geq 1\}$, we can solve $-\Delta \boldsymbol{\psi} = \boldsymbol{\omega}$ together with (2.9) to obtain $\{\boldsymbol{\psi}(x_i, y_j, z_k),\ i, j \in Z,\ k \geq 0\}$.

Next we come to the vorticity boundary conditions. The normal component of the vorticity $\omega_3|_\Gamma$ can be readily evaluated:

$$\omega_3(x, y, 0) = \left(\frac{\partial u_2}{\partial x} - \frac{\partial u_1}{\partial y}\right)(x, y, 0) = \left(\frac{\partial u_{2b}}{\partial x} - \frac{\partial u_{1b}}{\partial y}\right)(x, y). \tag{2.16}$$

The tangential components will be obtained from the tangential boundary conditions relating the velocity and vector potential:

$$\frac{\partial \psi_3}{\partial y} - \frac{\partial \psi_2}{\partial z} = u_{1b}, \quad \frac{\partial \psi_1}{\partial z} - \frac{\partial \psi_3}{\partial x} = u_{2b} \tag{2.17}$$

We approximate (2.17) by

$$(\tilde{D}_y \psi_3)(x_i, y_j, z_0) - \frac{\psi_2(x_i, y_j, z_1) - \psi_2(x_i, y_j, z_{-1})}{2\,\Delta z} = u_{1b}(x_i, y_j) \tag{2.18}$$

and

$$\frac{\psi_1(x_i, y_j, z_1) - \psi_1(x_i, y_j, z_{-1})}{2\,\Delta z} - (\tilde{D}_{x1} \psi_3)(x_i, y_j, z_0) = u_{2b}(x_i, y_j). \tag{2.19}$$

These formulas define $\{\psi_1(x_i, y_j, z_{-1}),\ i, j \in Z\}$ and $\{\psi_2(x_i, y_j, z_{-1}),\ i, j \in Z\}$:

$$\psi_2(x_i, y_j, z_{-1}) = \psi_2(x_i, y_j, z_1) - 2\,\Delta z((\tilde{D}_y \psi_3)(x_i, y_j, z_0) - u_{1b}(x_i, y_j)) \tag{2.20}$$

$$\psi_1(x_i, y_j, z_{-1}) = \psi_1(x_i, y_j, z_1) - 2\,\Delta z((\tilde{D}_x \psi_3)(x_i, y_j, z_0) + u_{2b}(x_i, y_j)). \tag{2.21}$$

Now we can evaluate ω_1, ω_2 at Γ:

$$\begin{aligned}
\omega_1(x_i, y_j, z_0) &= -(D_x^2 + D_y^2 + D_z^2)\psi_1(x_i, y_j, z_0) \\
&= -D_z^2 \psi_1(x_i, y_j, z_0) = -\frac{\psi_1(x_i, y_j, z_1) + \psi_1(x_i, y_j, z_{-1})}{\Delta z^2} \\
&= -\frac{2}{\Delta z^2}\psi_1(x_i, y_j, z_1) + \frac{2}{\Delta z}(\tilde{D}_x \psi_3(x_i, y_j, z_0) + u_{2b}(x_i, y_j)) \qquad (2.22) \\
\omega_2(x_i, y_j, z_0) &= -(D_x^2 + D_y^2 + D_z^2)\psi_2(x_i, y_j, z_0) \\
&= -D_z^2 \psi_2(x_i, y_j, z_0) = -\frac{\psi_2(x_i, y_j, z_1) + \psi_2(x_i, y_j, z_{-1})}{\Delta z^2} \\
&= -\frac{2}{\Delta z^2}\psi_2(x_i, y_j, z_1) + \frac{2}{\Delta z}(\tilde{D}_y \psi_3(x_i, y_j, z_0) - u_{1b}(x_i, y_j)). \qquad (2.23)
\end{aligned}$$

These are the analog of Thom's formula. This completes the description of the semi-discrete scheme.

As in 2D, variants of (2.22) and (2.23) can be derived. A fourth-order accurate one will be given in the Appendix.

For the fully discrete scheme it is important to treat the viscous terms explicitly. This point was discussed at length in [2]. Here we give the example of a forward Euler time stepping procedure. Notice that in practice, forward Euler is not suitable for even intermediate Reynolds number flows. This is also discussed in [2].

Given $\{\boldsymbol{\omega}^n_{i,j,k}\}_{k\geq 1}$, update $\{\boldsymbol{\omega}^{n+1}_{i,j,k}\}_{k\geq 1}$ by the following steps:

Step 1. Compute $\{\boldsymbol{\psi}^n_{i,j,k}\}_{k\geq 1}$ by solving

$$-\Delta_h \boldsymbol{\psi}^n = \boldsymbol{\omega}^n$$

with the boundary condition (2.15). Compute $\boldsymbol{u}^n$ via $\boldsymbol{u}^n = \tilde{\nabla}_h \times \boldsymbol{\psi}^n$.

Step 2. Evaluate the boundary vorticity using (2.16), (2.22)–(2.23).

Step 3. Compute $\{\boldsymbol{\omega}^{n+1}_{i,j,k}\}_{k\geq 1}$, using

$$\frac{\boldsymbol{\omega}^{n+1} - \boldsymbol{\omega}^n}{\Delta t} + \tilde{\nabla}_h \times (\boldsymbol{\omega}^n \times \boldsymbol{u}^n) = \nu \Delta_h \boldsymbol{\omega}^n.$$

It is straightforward to extend this to Runge–Kutta or multistep methods.

For convenience we will term this scheme Method A. Method B is a modification of Method A using the formulation in Proposition 2. Instead of using the Dirichlet boundary condition (2.16) for the normal component of vorticity, we impose the discrete divergence-free condition for vorticity at the grid points next to the boundary. This serves as a way of defining the values of the normal component of the vorticity at the boundary. Caution has to be exercised at the edges or corners since the normal component of the vorticity has been computed at more than one location at the boundary. In this case, we apply the discrete divergence-free condition several times using different stencils, with the centered difference being the last.

These methods are particularly simple and efficient for the case when the boundary of the domain consists of flat surfaces parallel to the coordinate planes. At every step or Runge–Kutta stage, only three separate scalar Poisson equations are solved. Moreover, standard fast Poisson solvers can be used.

3. ACCURACY TEST AND THE STRUCTURE OF THE ERROR

We can show that the methods presented in the last section are second-order accurate in velocity for smooth solutions. The details of the proofs will be presented elsewhere. From a numerical point of view it is much more informative to study the structure of the numerical error. Indeed a better way of discretizing the convective term will emerge from this study.

For our test problem, we choose the exact solution to be:

$$\boldsymbol{\psi}(\boldsymbol{x}, t) = e^t(\sin(\pi y)\sin(\pi z), \sin(\pi z)\sin(\pi x), \sin(\pi x)\sin(\pi y)) \quad \text{on } \Omega = [0, 1]^3 \quad (3.1)$$

and compute the velocity and vorticity from (3.1). For example,

$$\boldsymbol{\omega} = -\Delta \boldsymbol{\psi} = 2\pi^2 \boldsymbol{\psi}.$$

Clearly (3.1) gives a divergence-free vector potential. Appropriate forcing terms are added to the vorticity transport equation to make sure that (3.1) does give the exact solution. The boundary value of velocity is taken to be $\boldsymbol{u}_b = \nabla \times \boldsymbol{\psi}|_{\partial\Omega}$. Notice that $\boldsymbol{u}_b \cdot \boldsymbol{n} = 0$, so the complications from in-flow and out-flow boundaries do not arise here. This test solution is chosen for its simplicity. We will concentrate our discussion in this section on method B.

3.1. *Structure of the Error for the Unsteady Stokes Problem*

First we look at the unsteady Stokes equation. This allows us to concentrate on the effect of the vorticity boundary condition.

We verified numerically on 8^3, 16^3, and 32^3 grids that the method indeed has second-order accuracy and all the divergence-free conditions are satisfied very well. We will not present the numbers here since later on we will present them for the full Navier–Stokes equation. Instead we will look at the structure of error since this has an impact on our strategy for discretizing the nonlinear terms.

In Fig. 1a we plot the error in the numerical solution of ω_2 at the center plane $\{x = \frac{1}{2}\}$. It is clear that the error exhibits some peculiar feature at the boundary where the extension of Thom's formula (2.22)–(2.23) was used (see the following remark). When we compared the magnitude of the error at the interior and at the boundary over the whole cube, we found that the maximum error is not at the boundary. Furthermore, a similar phenomenon also occurs in 2D. This can be seen from Fig. 2, where we plot the error in vorticity computed by the 2D version of this method presented in [2] with the exact solution

$$\psi(\boldsymbol{x}, t) = e^t \sin(\pi x) \sin(\pi y). \tag{3.3}$$

This is done for the full Navier–Stokes equation. Both figures suggest that the error loses regularity at the boundary. For the linear problem, this phenomenon seems to be limited to the grid points at the boundary. To convince ourselves that this is not due to a loss of accuracy with Thom's formula, we plot in Fig. 2b the error for the 2D problem on the line $\{x = \frac{15}{32}\}$ and compare with the result when Thom's formula is replaced by Orszag–Israeli's formula [11]. We see that the formal higher order accuracy of Orszag–Israeli's formula has little effect on the error.

Remark. This special feature of the error in vorticity is due to the fact that a different formula (the 3D Thom's formula) is used to compute vorticity at the boundary. Therefore smoothness of the error is lost at the boundary. This is **not** a problem of numerical resolution at the boundary. No matter how resolved the numerical solution is, the error in vorticity will be of this form. This is true both in 2D and 3D.

3.2. *Discretization of the Nonlinear Term*

Having $\boldsymbol{\omega}$, and $\boldsymbol{u}$ (and hence $\boldsymbol{\omega} \times \boldsymbol{u}$) at all grid points, it is tempting to discretize $\nabla \times (\boldsymbol{\omega} \times \boldsymbol{u})$ by straightforward centered differences. However, since $\boldsymbol{\omega}_h$ has large jumps at the boundary when the vorticity boundary condition (2.22)–(2.23) is used,

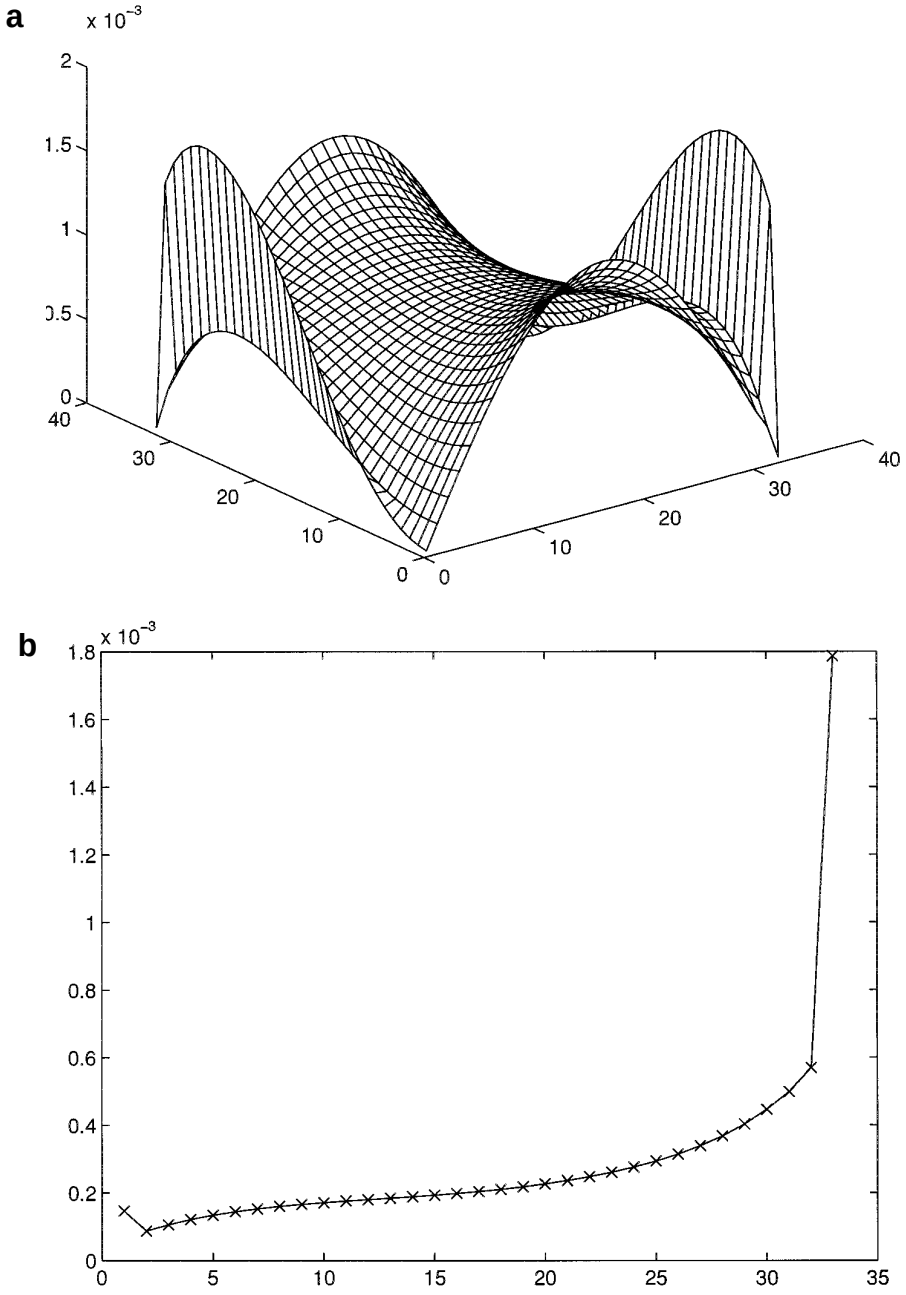

FIG. 1. (a) Numerical error in ω_2 at the center plane $\{x = \frac{1}{2}\}$ computed using Method B. Parameters: Re = 100, $t = 5$, $\Delta x = \frac{1}{32}$. (b) A cut of the quantity plotted in Fig. 1a at $\{y = \frac{15}{32}\}$.

we expect some problems with this approach. This is confirmed in Fig. 3, where we plot the error in ω_2 at the center plane $\{x = \frac{1}{2}\}$ for the full nonlinear problem. Not only that the loss of regularity has spread over to the interior, the accuracy in vorticity has reduced near the boundary.

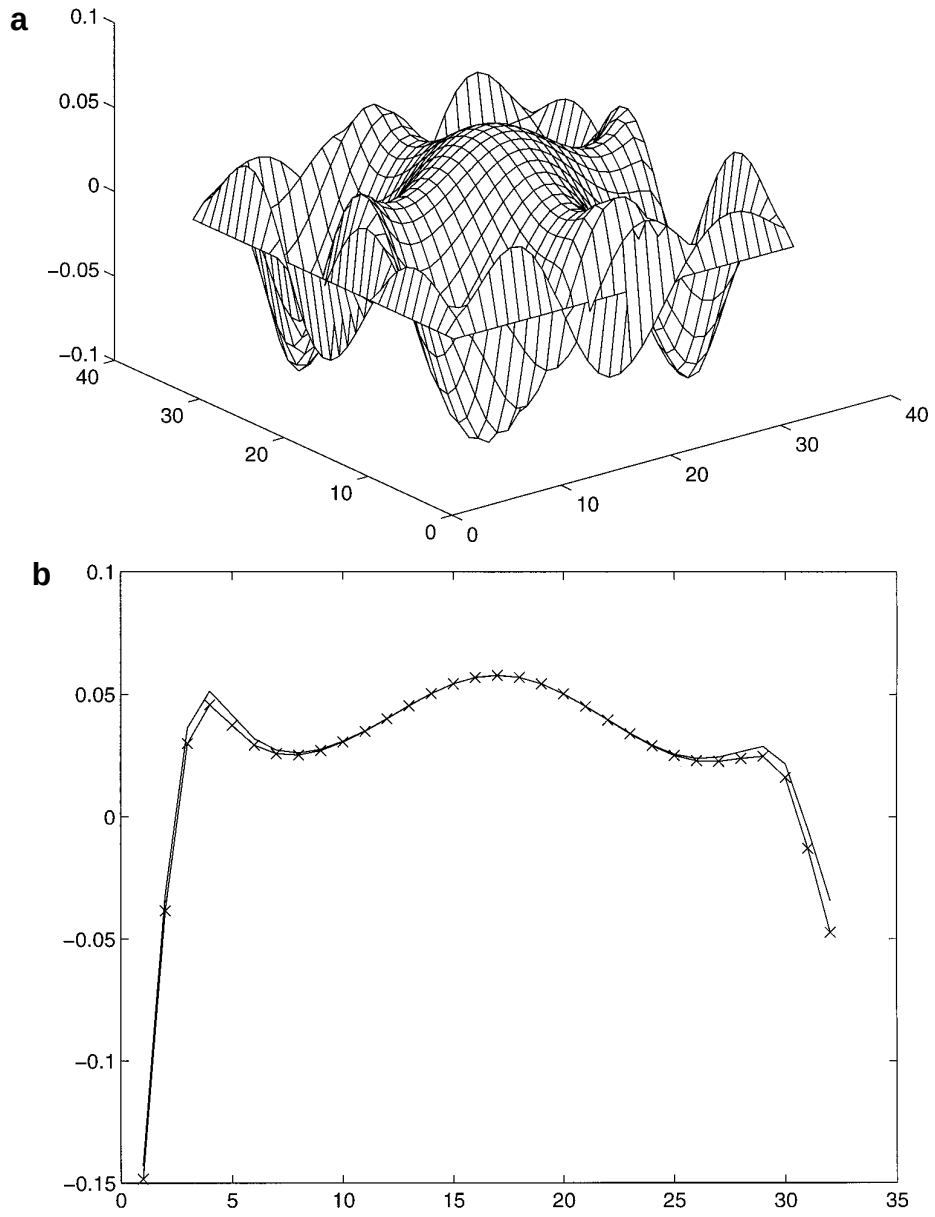

FIG. 2. (a) Numerical error in ψ in 2D for the full Navier–Stokes equation using a similar method and Thom's formula. Parameters: Re = 100, $t = 5$, $\Delta x = \frac{1}{32}$. (b) A cut of the quantity plotted in Fig. 2a at $\{x = \frac{15}{32}\}$, and comparison with the result when Thom's formula is replaced by Orszag–Israeli's formula.

The remedy for this is based on the following observation. The vorticity boundary condition of the type (2.22)–(2.23) was obtained through the no-slip boundary condition which is a consequence of the viscous term. For the convective term, however, the truly relevant boundary conditions are the ones associated with the Euler equation. In the present case, this is $\boldsymbol{u}_b \cdot \boldsymbol{n} = 0$. Therefore, instead of using Thom's formula to evaluate $\boldsymbol{\omega} \times \boldsymbol{u}$, we should use

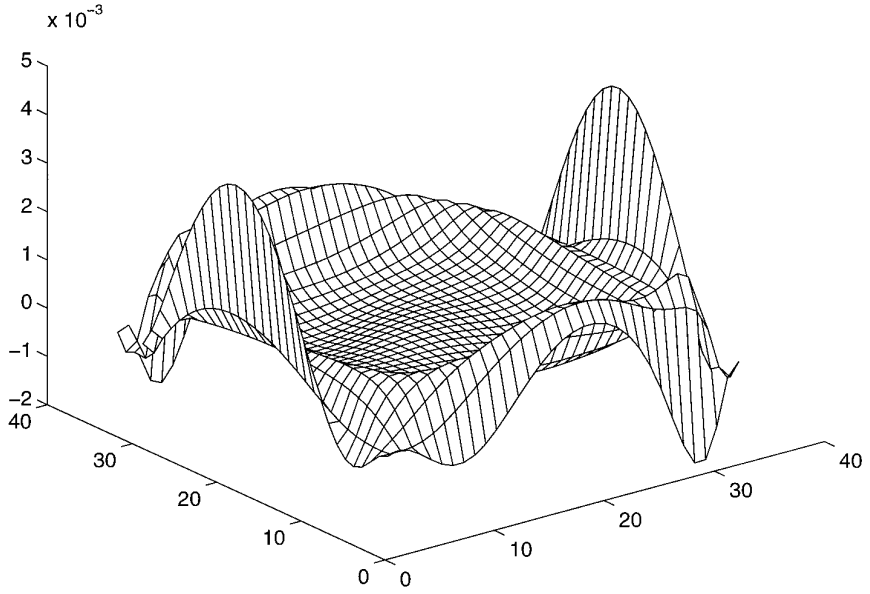

FIG. 3. Numerical error in vorticity ω_2 at the center plane $\{x = \frac{1}{2}\}$ computed using Method B for the full nonlinear problem. Thom's formula is used for the convective term. Parameters: Re = 100, $t = 5$, $\Delta x = \frac{1}{32}$.

$$\boldsymbol{\omega} \times \boldsymbol{u} = (\nabla \times \boldsymbol{u}) \times \boldsymbol{u} = (\nabla \times (\nabla \times \boldsymbol{\psi})) \times \nabla \times \boldsymbol{\psi} \tag{3.4}$$

computed through the vector potential. Since the vector potential does not use the vorticity boundary values computed through Thom's formula, the problem described in Section 3.1 will not seriously influence $\boldsymbol{\omega} \times \boldsymbol{u}$ if it is computed using (3.4). Note that a one-sided difference is needed to evaluate (3.4) at the boundary.

In Fig. 4 we plot the same quantity as in Fig. 3, except the nonlinear term is evaluated at the interior grid points according to (3.4). We see that the error has a very similar structure as in Fig. 1, and the loss of regularity is limited to grid points at the boundary.

The second-order accuracy of this method can be read from Table I. Two more conclusions are suggested by Table I. The first is that the divergence conditions are satisfied with remarkable accuracy. The second is that the error at the boundary is not larger than the error in the interior.

4. THE CUBIC DRIVEN CAVITY FLOW

In this section we report our numerical results on applying Method B to a standard test problem: the driven cavity flow. We will also compare with the results of the MAC scheme since this is an ideal situation for the MAC scheme. Results from Method A will be reported in the next section.

The setup of the problem is the following: The flow is limited to a cubic cavity $[0, 1]^3$ and the upper lid of the cavity at $\{y = 1\}$ moves with velocity $\boldsymbol{u}_b = (1, 0, 0)$.

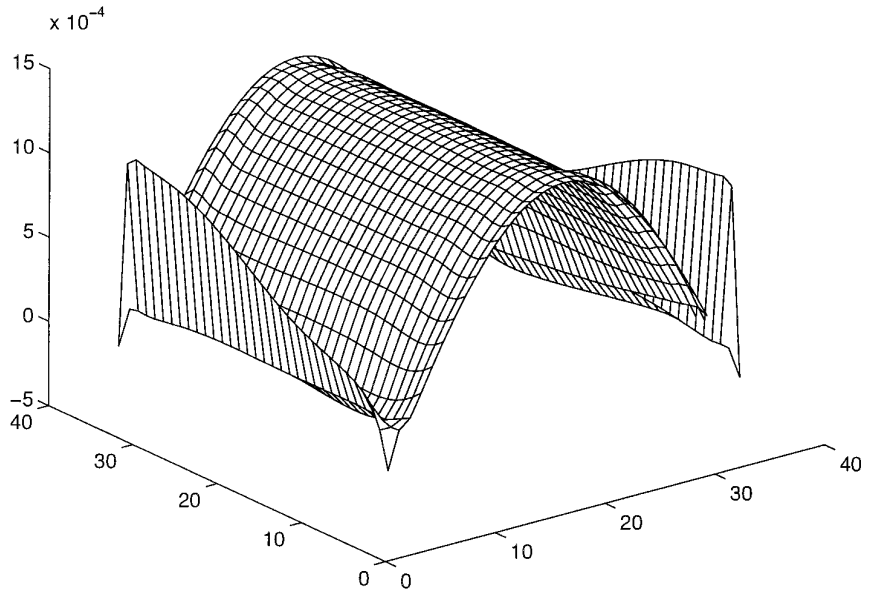

FIG. 4. Numerical error in ω_2 at the center plane $\{x = \frac{1}{2}\}$ computed using Method B for the full nonlinear problem, using (3.4). Parameters: Re = 100, $t = 5$, $\Delta x = \frac{1}{32}$.

There is an extensive literature on this problem, both experimental and numerical. Much of the book [1] is devoted to the numerical simulation of the driven cavity flow with length to width to height aspect ratio 3 : 1 : 1 at Reynolds number 3200 and with impulsive start. While most of the numerical results reported in [1] have some qualitative agreement with the experimental results of Koseff and Street [9], there was very little agreement in the quantitative aspects such as the number of Taylor–Gorter vortices. In this paper we will show results of three different numerical methods with reasonable agreement.

This is a tough test for the methods proposed in this paper since vorticity becomes singular at the upper edges at infinite Reynolds number. We found it representative

TABLE I

	8^3	16^3	32^3
$\dfrac{\|\boldsymbol{u} - \boldsymbol{u}_h\|_\infty}{h^2\|\boldsymbol{u}\|_\infty}$	0.067930	0.064274	0.076920
$\dfrac{\|\boldsymbol{\omega} - \boldsymbol{\omega}_h\|_\infty}{h^2\|\boldsymbol{\omega}\|_\infty}$	2.386185	2.516361	2.551321
$\dfrac{\|\boldsymbol{\omega} - \boldsymbol{\omega}_h\|_{\infty,\Gamma}}{h^2\|\boldsymbol{\omega}\|_{\infty,\Gamma}}$	1.449268	1.546228	1.976430
$\|\text{div } \boldsymbol{\omega}_h\|_\infty$	1.716613E-4	2.021789E-4	4.575247E-4
$\|\text{div } \psi_h\|_\infty$	2.205371E-4	7.236003E-5	2.071153E-5
$\dfrac{\|\text{div } \boldsymbol{u}_h\|_\infty}{h^2}$	3.814697E-6	7.629394E-6	1.364224E-12

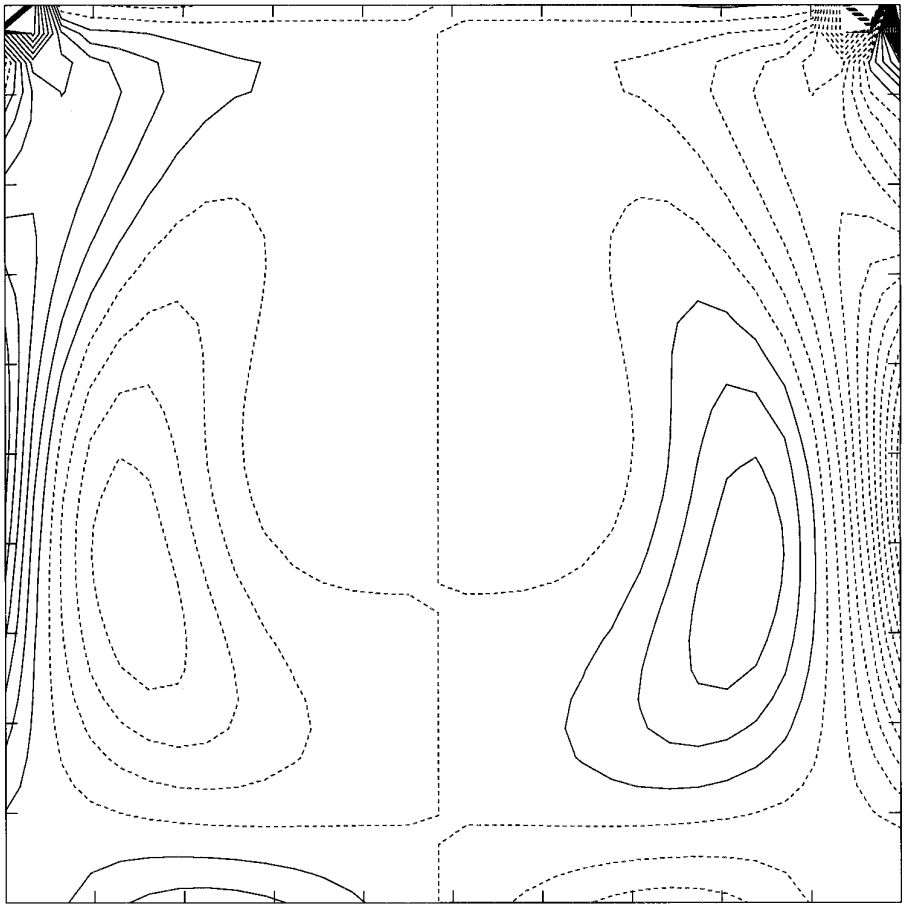

FIG. 5. Contour plot of ω_1 at the center plane $\{x = \frac{1}{2}\}$ computed using Method B. Parameters: Re = 500, $t = 20$, $CFL = \Delta t/\Delta x = 2.5$, $\Delta x = \frac{1}{32}$.

to report the results on the longitudinal vorticity component at the center plane. Figure 5 is the contour plot of ω_1 at Reynolds number 500. This should be compared to Fig. 6, where we plot the same quantity as in Fig. 5 computed using the MAC scheme based on the primitive variables. Except for some details, the agreement is quite reasonable. At this low Reynolds number, the flow converges to steady state.

Among the details that the two methods disagree is the behavior at the corners where the flow becomes singular. In Fig. 7 we plot ω_2 at the center plane computed using Method B. We can see clearly traces of the classical Gibbs phenomenon. At Reynolds number 500, the numerical results were still reasonably accurate despite the Gibbs phenomenon. At higher Reynolds numbers (say 1600 or 3200) we found that the numerical solutions computed using Method B on a 64^3 grid differs greatly from the ones computed using the MAC scheme on the same grid. As an example of the solutions computed using the MAC scheme we display in Fig. 8 the contour plot of ω_1 at the center plane at $t = 15$ and Reynolds number 3200. We verified that this agrees quite well with the numerical solution on a 128^3 grid.

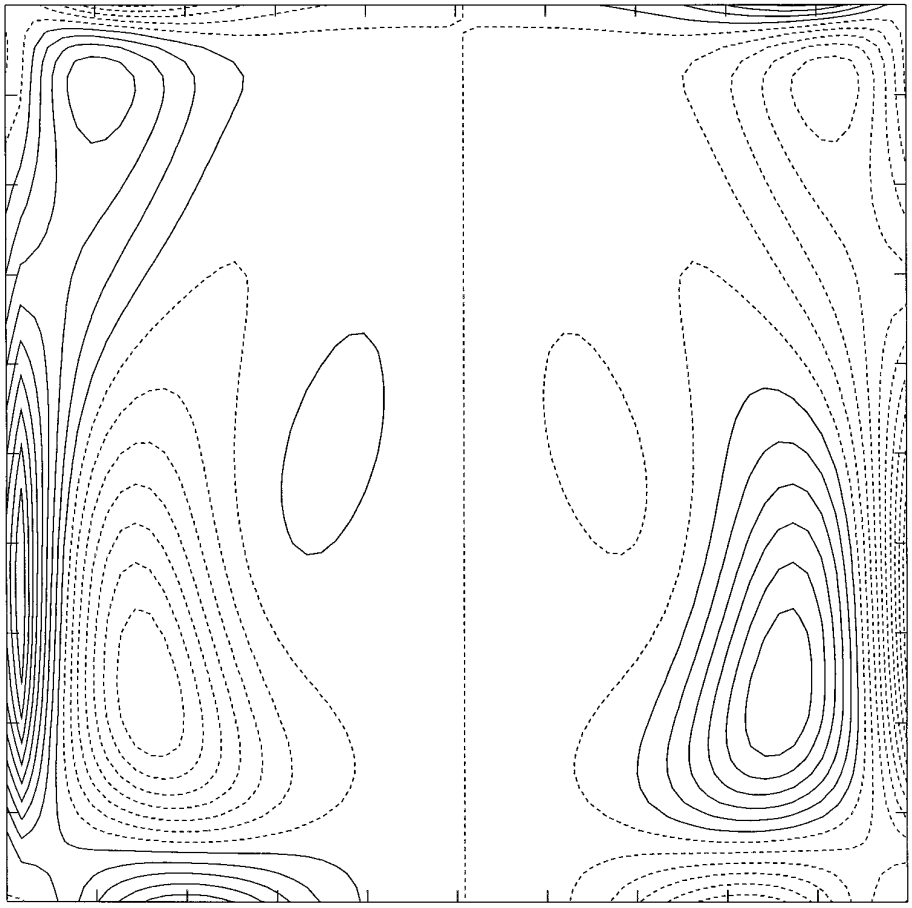

FIG. 6. Contour plot of ω_1 at the center plane $\{x = \frac{1}{2}\}$ computed using MAC scheme. Parameters: Re = 500, $t = 20$, $CFL = \Delta t/\Delta x = 2.5$, $\Delta x = \frac{1}{32}$.

It is still a bit of a mystery that the Gibbs phenomena and the associated problem with slow convergence at high Reynolds numbers can be eliminated by simply using

$$\nabla \times (\boldsymbol{\omega} \times \boldsymbol{u}) \doteq \nabla_h \times ((\boldsymbol{u} \cdot \nabla)\boldsymbol{u}). \tag{4.1}$$

The effect of this alternative approach for computing the nonlinear term is seen in Fig. 9, where we show the same result as in Fig. 7 after using (4.1). We see that the Gibbs phenomenon has disappeared. To see that this has more than cosmetic values we present in Fig. 10 the results of Method B with (4.1) at $t = 15$ and Reynolds number 3200 on a 64^3 grid. Considering that this is a rather coarse grid for this Reynolds number, the agreement between Figs. 10 and 8 are quite satisfactory.

From a physical point of view, what is interesting about these flows is the appear-

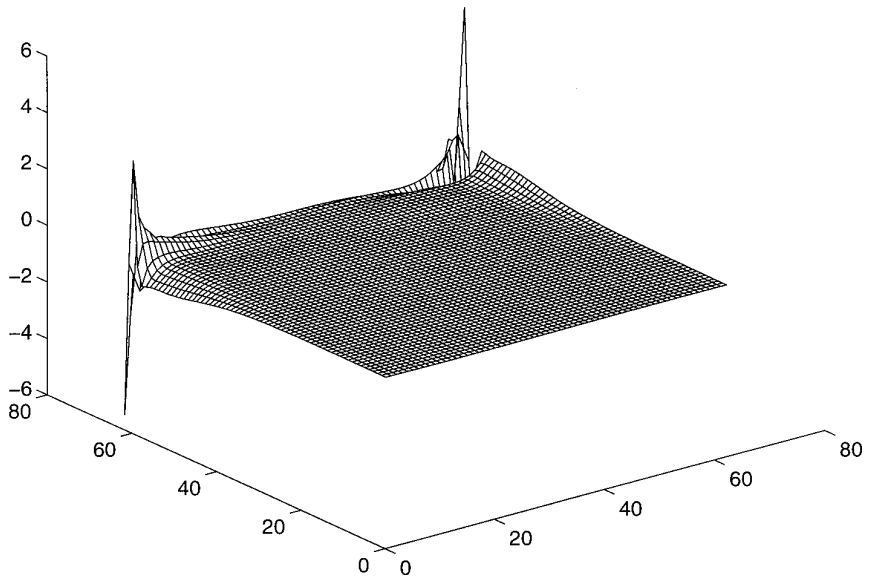

FIG. 7. ω_2 at the center plane $\{x = \frac{1}{2}\}$ computed using Method B. Parameters: Re = 500, $t = 20$, $CFL = \Delta t/\Delta x = 2.5$, $\Delta x = \frac{1}{32}$.

ance of Taylor–Gorter vortices. These are the quadrupolar vortices that develop at the boundary of the primary and secondary vortices as a result of an instability analogous to the one seen in Taylor–Couette flow.

5. METHOD A AND THE DIVERGENCE-FREE CONDITION FOR VORTICITY

Compared with Method B, Method A has the feature that the vorticity boundary condition is very easy to implement. It also enforces the divergence free condition for vorticity much more indirectly. The effect of this is the subject of this section.

5.1. *Accuracy Test for Smooth Solutions*

We first report the results of the accuracy test for the smooth solutions used in Section 3. The results are summarized in Table II. Several things can be learned from Table II. The first is that the divergence-free condition for vorticity and vector potential is much more poorly approximated than in Method B. On a 16^3 grid the divergence of vorticity in maximum norm is about 1.36. This is quite large considering how simple the exact solution is. To make sure that this is not a problem limited at the boundary, we plot in Fig. 11 the numerically computed divergence of vorticity at the center plane. Although the maximum occurs at the boundary, the divergence is not anomolously high there, compared with its values in the interior.

The second conclusion is that the divergence-free conditions do seem to be satisfied with second-order accuracy. It is just that the constants of proportionality can be rather big.

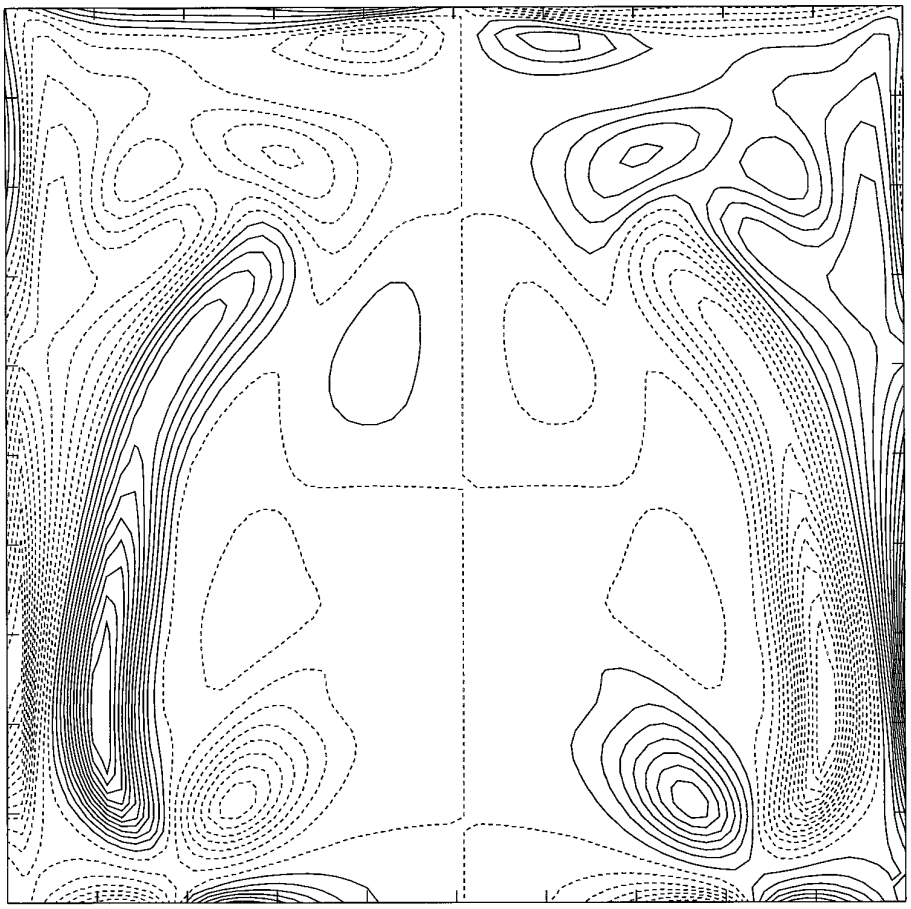

FIG. 8. Contour plot of ω_1 at the center plane $\{x = \frac{1}{2}\}$ computed using MAC scheme. Parameters: Re = 3200, $t = 15$, $CFL = \Delta t/\Delta x = 2.5$, $\Delta x = \frac{1}{64}$.

The third conclusion is that despite the fact that the divergence-free condition for vorticity is poorly approximated, the overall accuracy for velocity and vorticity is still second order. In fact the accuracy in these quantities is comparable with that of Method B.

The explanation lies in that for Method A, divergence-free conditions for vorticity and vector potential are enforced through approximation results. Since the divergence is a quantity involving derivatives, and since derivatives are usually less accurate than the function values, we expect that the divergence-free condition in vorticity is less accurately approximated than vorticity itself. The same can be said for vector potential but the effect is less drastic.

5.2. *The Driven Cavity Flow*

Method A can be used equally well for the driven cavity flow, both for the lower (Re = 500) and higher (Re = 3200) Reynolds number cases. These results are

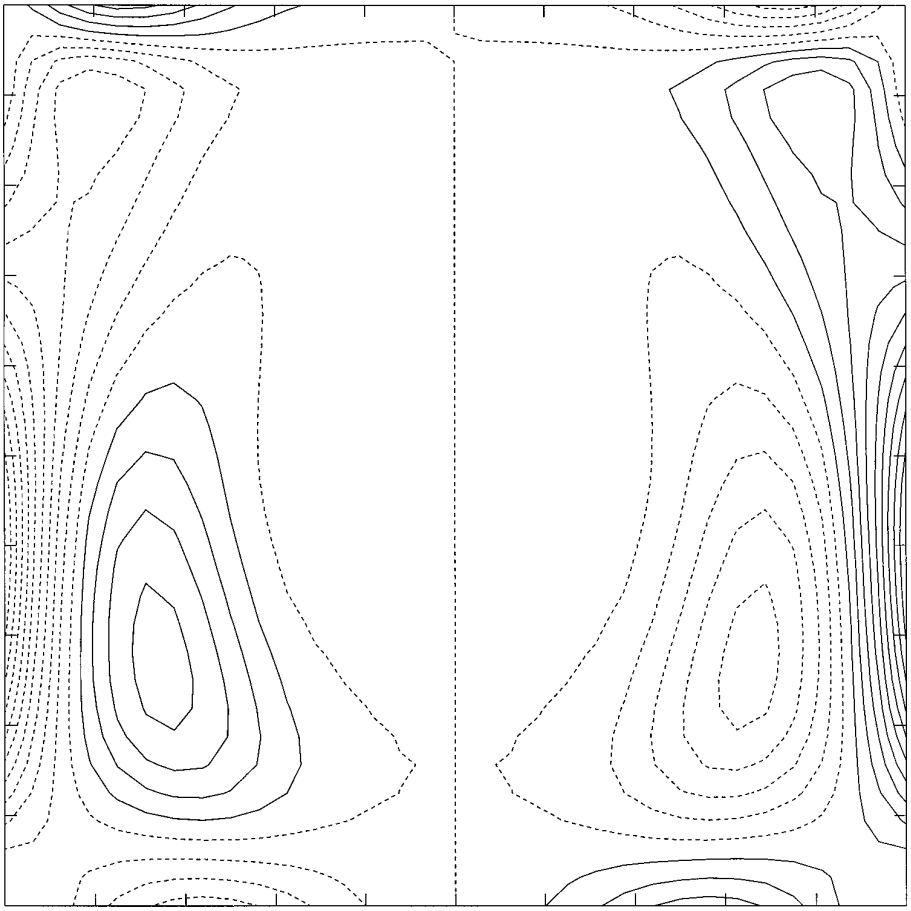

FIG. 9. Contour plot of ω_1 at the center plane $\{x = \frac{1}{2}\}$ computed using Method B and (4.1). Parameters: Re = 500, $t = 20$, $CFL = \Delta t/\Delta x = 2.5$, $\Delta x = \frac{1}{32}$.

shown in Figs. 12–13. Here we used (4.1) to compute the nonlinear terms. Since the flow is singular at the upper edges, the divergence of vorticity is very poorly approximated there. In fact the maximum value of the computed divergence of vorticity was about 288 for Re = 500 and 3000 for Re = 3200. These large values are limited to the upper edges. Still the overall quality of the numerical solution is comparable to the ones computed using MAC scheme or Method B.

6. CONCLUDING REMARKS

Let us reiterate the important aspects of the methods proposed in this paper:

1. This method seems to be the first working finite difference method on nonstaggered grids in vorticity form. In terms of complexity, this method is comparable

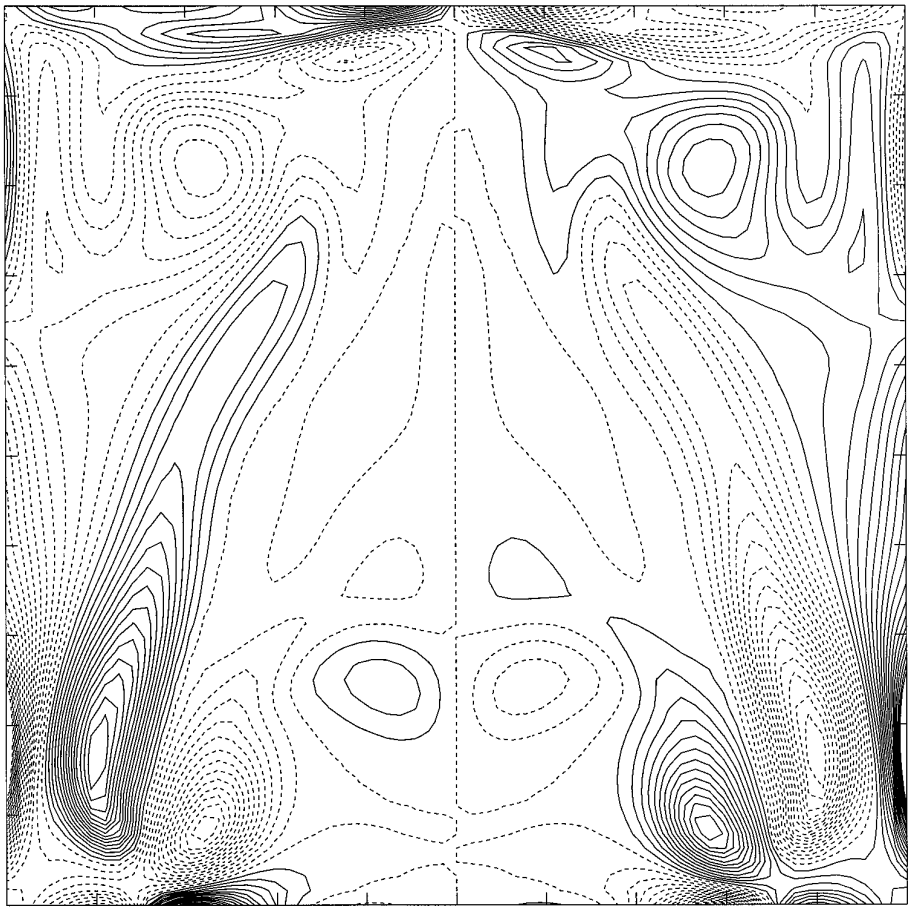

FIG. 10. Contour plot of ω_1 at the center plane $\{x = \frac{1}{2}\}$ computed using Method B and (4.1). Parameters: Re = 3200, $t = 15$, $CFL = \Delta t/\Delta x = 2.5$, $\Delta x = \frac{1}{64}$.

with standard finite difference methods for Poisson equations. Although we made the comparisons with the MAC scheme in a cubic geometry, the real advantage of this method is its flexibility with more complicated geometry when staggered grid becomes prohibitively complex.

2. The error structure in vorticity for such methods has a distinct form at the boundary. This may seem surprising at a first glance. But this is just a consequence of the fact that a difference formula is used to compute vorticity at the boundary.

APPENDIX 1: COMPACT FOURTH-ORDER SCHEME

In [3], we introduced an essentially compact fourth-order (EC4 for short) finite difference scheme for 2D problems based on the ω-ψ formulation and demonstrated its clear superiority over the second-order scheme. In this Appendix we extend

TABLE II

	16^3	32^3
$\frac{\|\boldsymbol{u}-\boldsymbol{u}_h\|_\infty}{h^2\|\boldsymbol{u}\|_\infty}$	0.245454	0.274226
$\frac{\|\boldsymbol{\omega}-\boldsymbol{\omega}_h\|_\infty}{h^2\|\boldsymbol{\omega}\|_\infty}$	3.158329	3.214455
$\frac{\|\boldsymbol{\omega}-\boldsymbol{\omega}_h\|_{\infty,\Gamma}}{h^2\|\boldsymbol{\omega}\|_{\infty,\Gamma}}$	2.031312	3.441604
$\|\text{div } \boldsymbol{\omega}_h\|_\infty$	1.360162	0.389763
$\|\text{div } \boldsymbol{\omega}_h\|_{L_1}$	0.428908	0.126301
$\|\text{div } \boldsymbol{\psi}_h\|_\infty$	0.015103	0.003832
$\|\text{div } \boldsymbol{\psi}_h\|_{L_1}$	0.004833	0.001255
$\|\text{div } \boldsymbol{u}_h\|_\infty$	4.547473E-13	1.364242E-12
$\|\text{div } \boldsymbol{u}_h\|_{L_1}$	5.606105E-14	1.468645E-13

EC4 to 3D problems. We will limit our discussion to Method A. Extension to Method B is immediate.

As in [3] we will delay the treatment of the convection term and write it as $\boldsymbol{f} = \nabla \times (\boldsymbol{\omega} \times \boldsymbol{u})$. The basic strategy is the same as in standard fourth-order compact schemes. For simplicity of presentation we will first treat the case when $\Delta x = \Delta y = \Delta z = h$ and indicate the changes required for the general case later. We approximate

$$\frac{\partial \boldsymbol{\omega}}{\partial t} = \nu \Delta \boldsymbol{\omega} - \boldsymbol{f} \tag{A.1}$$

to fourth-order via

$$\left(1 + \frac{h^2}{12}\Delta_h\right)\frac{\partial \boldsymbol{\omega}}{\partial t} = \nu\left(\Delta_h + \frac{h^2}{6}(D_x^2 D_y^2 + D_y^2 D_z^2 + D_z^2 D_x^2)\right)\boldsymbol{\omega} - \left(1 + \frac{h^2}{12}\Delta_h\right)\boldsymbol{f} \tag{A.2}$$

and approximate $-\Delta \boldsymbol{\psi} = \boldsymbol{\omega}$ to fourth-order via

$$-\left(\Delta_h + \frac{h^2}{6}(D_x^2 D_y^2 + D_y^2 D_z^2 + D_z^2 D_x^2)\right)\boldsymbol{\psi} = \left(1 + \frac{h^2}{12}\Delta_h\right)\boldsymbol{\omega}. \tag{A.3}$$

We supplement (A.3) with the boundary condition (2.15).

(A.2) needs the boundary values of $\boldsymbol{\omega}$. For ω_3 this is easy,

$$\omega_3 = \frac{\partial u_{2b}}{\partial x} - \frac{\partial u_{1b}}{\partial y} \quad \text{on } \Gamma.$$

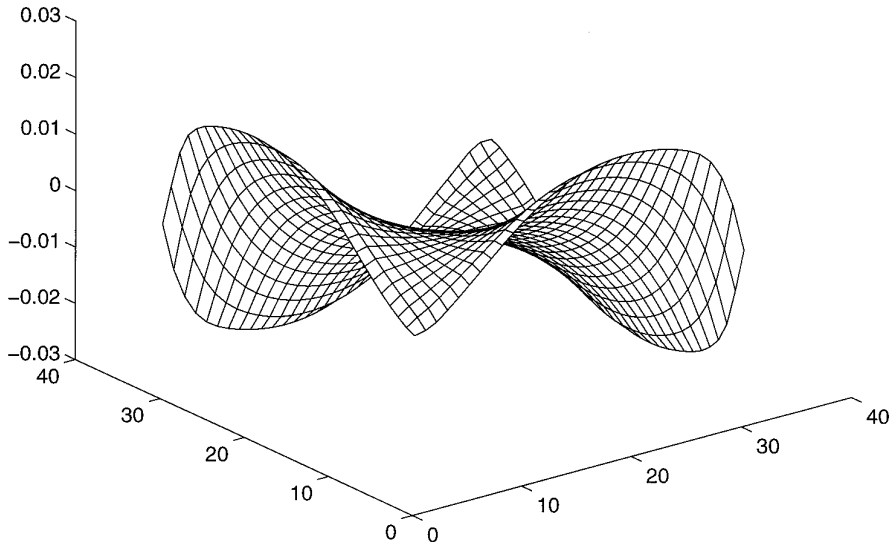

FIG. 11. Discrete divergence of vorticity ω_2 at the center plane $\{x = \frac{1}{2}\}$ for the smooth test problem computed using Method A for the linear problem. Parameters: Re = 100, $t = 5$, $\Delta x = \frac{1}{32}$.

The easiest way to obtain the boundary values of ω_1 and ω_2 is to define $\boldsymbol{\psi}$ on two lines of "ghost points" $\{(x_i, y_j, z_{-1}), (x_i, y_j, z_{-2}), i, j \in Z, z_{-1} = -\Delta z, z_{-2} = -2\,\Delta z\}$ by using (2.17) twice at the physical boundary Γ: once using a fourth-order one-sided approximation, once using a fourth-order centered approximation. Omitting the x_i, y_j variables, we can write

$$\left(\frac{\partial \psi_2}{\partial z}\right)\bigg|_\Gamma \approx \frac{-3\psi_2(z_{-1}) - 10\psi_2(z_0) + 18\psi_2(z_1) - 6\psi_2(z_2) + \psi_2(z_3)}{12h}$$

$$\left(\frac{\partial \psi_2}{\partial z}\right)\bigg|_\Gamma \approx \frac{\psi_2(z_{-2}) - 8\psi_2(z_{-1}) + 8\psi_2(z_1) - \psi_2(z_2)}{12h}.$$

Similarly for ψ_1. Together with (2.17) we get

$$\psi_2(z_{-1}) = 6\psi_2(z_1) - 2\psi_2(z_2) + \tfrac{1}{3}\psi_2(z_3) - 4h\left(\frac{\partial \psi_3}{\partial y} - u_{1b}\right)(z_0)$$

$$\psi_2(z_{-2}) = 40\psi_2(z_1) - 15\psi_2(z_2) + \tfrac{8}{3}\psi_2(z_3) - 12h\left(\frac{\partial \psi_3}{\partial y} - u_{1b}\right)(z_0)$$

$$\psi_1(z_{-1}) = 6\psi_1(z_1) - 2\psi_1(z_2) + \tfrac{1}{3}\psi_1(z_3) - 4h\left(\frac{\partial \psi_3}{\partial x} + u_{2b}\right)(z_0)$$

$$\psi_1(z_{-2}) = 40\psi_1(z_1) - 15\psi_1(z_2) + \tfrac{8}{3}\psi_1(z_3) - 12h\left(\frac{\partial \psi_3}{\partial x} + u_{2b}\right)(z_0).$$

To evaluate ω_1, ω_2 at the boundary, we use a fourth-order approximation of $\boldsymbol{\omega}$,

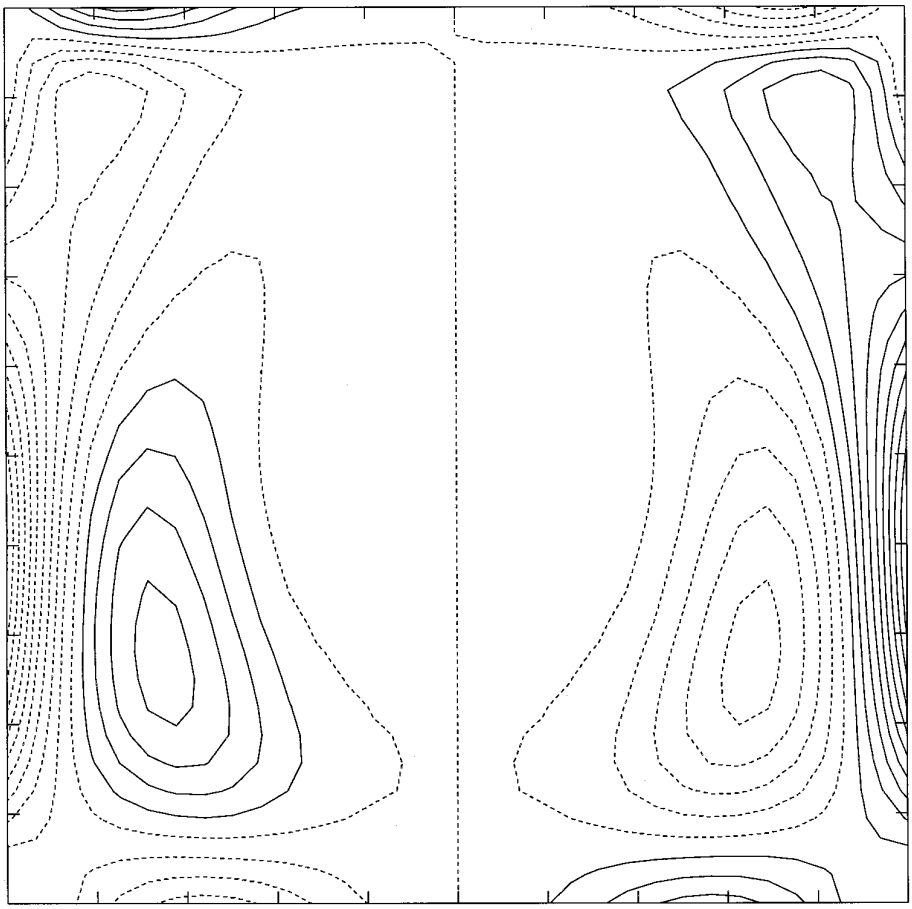

FIG. 12. Contour plot of ω_1 at the center plane $\{x = \frac{1}{2}\}$ computed using Method A and (4.1). Parameters: Re = 500, $t = 20$, $CFL = \Delta t/\Delta x = 2.5$, $\Delta x = \frac{1}{32}$.

$$\omega_2|_\Gamma = \frac{108\psi_2(z_1) - 27\psi_2(z_2) + 4\psi_2(z_3)}{18h^2} - \frac{11}{3h}\left(\frac{\partial \psi_3}{\partial y} - u_{1b}\right)(z_0)$$

$$\omega_1|_\Gamma = \frac{108\psi_1(z_1) - 27\psi_1(z_2) + 4\psi_1(z_3)}{18h^2} - \frac{11}{3h}\left(\frac{\partial \psi_3}{\partial x} + u_{2b}\right)(z_0).$$

These can be readily evaluated by approximating $\partial\psi_3/\partial x$, $\partial\psi_3/\partial y$ on Γ using standard fourth-order formulas.

To treat the convection terms, we note that

$$\left(1 + \frac{h^2}{12}\Delta_h\right)\tilde{D}_x\left(1 - \frac{h^2}{6}D_x^2\right) = \tilde{D}_x\left(1 + \frac{h^2}{6}(D_y^2 + D_z^2)\right) - \frac{h^2}{12}\Delta_h\tilde{D}_x + O(h^4).$$

Therefore we can approximate $(1 + (h^2/12)\,\Delta_h)\boldsymbol{f}$ to fourth order using

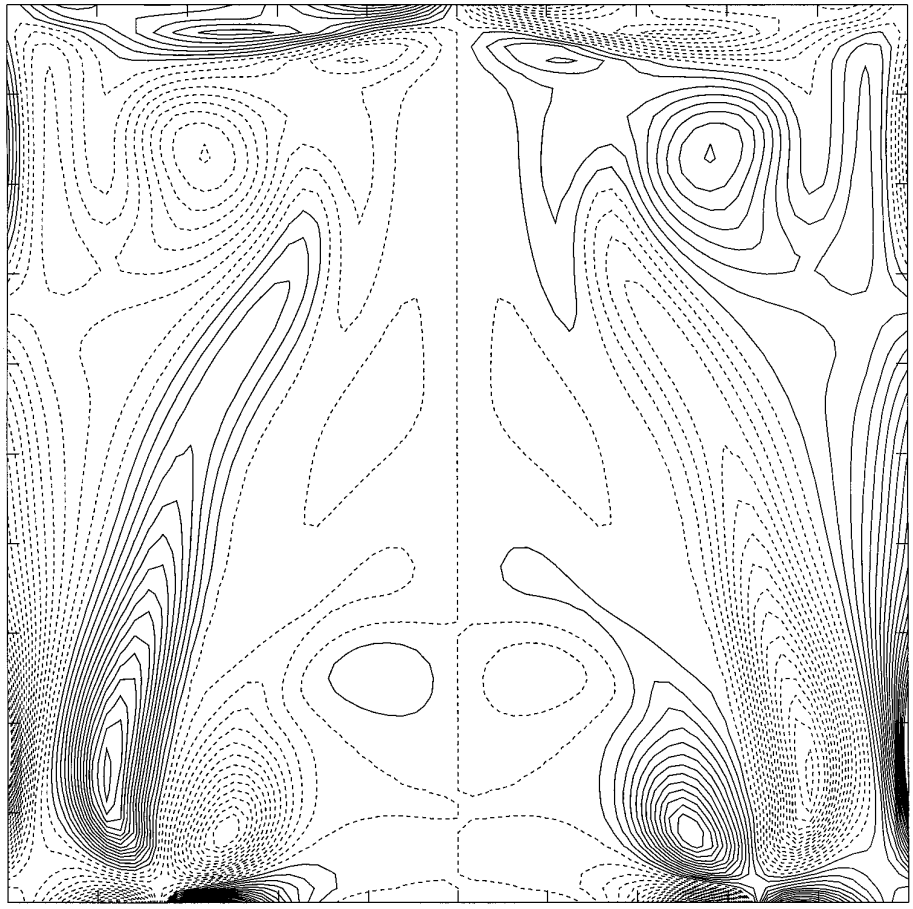

FIG. 13. Contour plot of ω_1 at the center plane $\{x = \frac{1}{2}\}$ computed using Method A and (4.1). Parameters: Re = 3200, $t = 15$, $CFL = \Delta t/\Delta x = 2.5$, $\Delta x = \frac{1}{64}$.

$$\left(1 + \frac{h^2}{12}\Delta_h\right)\boldsymbol{f}$$

$$= \left(1 + \frac{h^2}{12}\Delta_h\right)\nabla \times (\boldsymbol{\omega} \times \boldsymbol{u})$$

$$= \left(\tilde{D}_x\left(1 + \frac{h^2}{6}(D_y^2 + D_z^2)\right), \tilde{D}_y\left(1 + \frac{h^2}{6}(D_x^2 + D_z^2)\right), \tilde{D}_z\left(1 + \frac{h^2}{6}(D_x^2 + D_y^2)\right)\right)$$

$$\times (\boldsymbol{\omega} \times \boldsymbol{u}) - \frac{h^2}{12}\Delta_h\tilde{\nabla}_h \times (\boldsymbol{\omega} \times \boldsymbol{u}) + O(h^4).$$

The first term in the right-hand side involves only compact difference formulas. The second term can be rewritten as

$$-\frac{h^2}{12}\Delta_h((\boldsymbol{u}\cdot\tilde{\nabla}_h)\boldsymbol{\omega} - (\boldsymbol{\omega}\cdot\tilde{\nabla}_h)\boldsymbol{u}) + O(h^4).$$

This is not compact and requires the boundary value of $(\boldsymbol{u}\cdot\tilde{\nabla}_h)\boldsymbol{\omega} - (\boldsymbol{\omega}\cdot\tilde{\nabla}_h)\boldsymbol{u}$. There is a very natural way of assigning this boundary value. On Γ

$$(\boldsymbol{u}\cdot\tilde{\nabla}_h)\boldsymbol{\omega} = u_{1b}\tilde{D}_x\boldsymbol{\omega} + u_{2b}\tilde{D}_y\boldsymbol{\omega}$$

which can be readily evaluated since $\boldsymbol{\omega}$ is known on Γ. We also have

$$\nabla\boldsymbol{u} = \begin{pmatrix} \dfrac{\partial u_{1b}}{\partial x} & \dfrac{\partial u_{2b}}{\partial x} & 0 \\ \dfrac{\partial u_{1b}}{\partial y} & \dfrac{\partial u_{2b}}{\partial y} & 0 \\ \omega_2 & -\omega_1 & -\left(\dfrac{\partial u_{1b}}{\partial x} + \dfrac{\partial u_{2b}}{\partial y}\right) \end{pmatrix}.$$

Therefore, numerically we can approximate $(\boldsymbol{\omega}\cdot\nabla)\boldsymbol{u}$ to second order using

$$\tilde{\nabla}_h\boldsymbol{u} = \begin{pmatrix} \tilde{D}_x u_{1b} & \tilde{D}_x u_{2b} & 0 \\ \tilde{D}_y u_{1b} & \tilde{D}_y u_{2b} & 0 \\ \omega_2 & -\omega_1 & -(\tilde{D}_x u_{1b} + \tilde{D}_y u_{2b}) \end{pmatrix}.$$

The matrix on the right-hand side can be readily evaluated. This completes the description of the semidiscrete scheme.

This scheme is termed essentially compact for obvious reasons. It has all the advantages of a compact with regard to accuracy and boundary conditions. The description of the fully discrete scheme is the same as in 2D [3]. We omit the details.

APPENDIX 2: IN-FLOW AND OUT-FLOW BOUNDARY CONDITIONS

We now describe the in-flow and out-flow boundary conditions. For simplicity, we discuss the case of flow in a duct $[0, 10] \times [0, 1]^2$. The no-flow and no-slip boundary condition is imposed at the side of the duct. At the inlet and outlet, we impose the in-flow and out-flow boundary condition. As we discussed before, at the side, we take the Dirichlet–Neumann boundary condition (2.8). At the inlet say at $x = 0$, we specify $\boldsymbol{u}$. At the outlet, we impose $\partial_x\boldsymbol{u} = 0$.

Part of (2.8) now has to be changed as follows. At the inlet ($x = 0$, $(y, z) \in [0, 1]^2$) or the outlet ($x = 10$, $(y, z) \in [0, 1]^2$)), we impose:

$$\partial_x\psi_1 = 0 \tag{A.4}$$

and

$$\partial_y\psi_2 + \partial_z\psi_3 = 0. \tag{A.5}$$

In order to impose the boundary condition of (A.5), we introduce $\Phi(y, z)$ such that

$$\psi_2 = -\partial_z \Phi, \quad \psi_3 = \partial_y \Phi. \tag{A.5}$$

Using relation

$$u_1 = \partial_y \psi_3 - \partial_z \psi_2 = -\Delta_{y,z} \Phi$$

on the boundary $y = 0, 1$ ($z = 0, 1$), we naturally impose the Neumann boundary condition $\partial_z \Phi = 0$ ($\partial_y \Phi = 0$). This is consistent with $\psi_3 = 0$ ($\psi_2 = 0$). In summary, we first solve

$$\begin{aligned} &-\Delta_{y,z} \Phi = u_1|_{x=0,10}(y, z) && \text{for } 0 < y, z < 1, \\ &\partial_n \Phi = 0 && \text{on } y = 0, 1, \text{ or } z = 0, 1 \end{aligned} \tag{A.6}$$

and then find ψ_2 and ψ_3 on the inlet and outlet boundaries from relation (A.5).

The idea was explained in [3] for the 2D cases and implemented for flow passing a backward facing step.

REFERENCES

1. M. Deville, T. H. Lê, and Y. Morchoisne (Eds.), *Numerical Simulation of 3-D Incompressible Unsteady Viscous Laminar Flows*, Notes on Numerical Fluid Mechanics, Vol. 36, (1992), Brauschweig, F. Vieweg.
2. W. E and J.-G. Liu, Vorticity boundary condition and related issues for finite difference schemes, *J. Comput. Phys.* **124,** 368 (1996).
3. W. E and J.-G. Liu, Essentially compact schemes for unsteady viscous incompressible flows, *J. Comput. Phys.* **125,** 122 (1966).
4. W. E and J.-G. Liu, Finite difference methods for viscous incompressible flows in vorticity formulations, in *ESAIM: Proceedings, 1996*, Vol. 1, p. 181. [http://www.emath.fr/proc/Vol.1/]
5. F. H. Harlow and J. E. Welch, Numerical calculation of time-dependent viscous incompressible flow of fluid with free surface, *Phys. Fluids* **8,** 2182 (1965).
6. U. Ghia, K. N. Ghia, and C. T. Shin, High-Re solutions of incompressible flow using the Navier–Stokes equations and a multi-grid method, *J. Comput. Phys.* **48** (1982).
7. P. M. Gresho, Some interesting issues in incompressible fluid dynamics, both in the continuum and in numerical simulation, *Adv. Appl. Mech.* **28,** 45 (1992).
8. G. Guj and F. Stella, A vorticity-velocity method for the numerical solution of 3D incompressible flows, *J. Comput. Phys.* **106,** 286 (1993).
9. J. R. Koseff and R. L. Street, Visualization studies of a shear driven 3-D recirculating flow, *J. Fluids Eng.* **106,** 21 (1984).
10. R. A. Nicolaides, in Incompressible Computational Fluid Dynamics, edited by Gunzburger and Nicolaides (Cambridge Univ. Press, Cambridge, 1993).
11. S. A. Orzag and M. Israeli, Numerical simulation of viscous incompressible flow, *Annu. Rev. Fluid Mech.* **6,** 281 (1974).
12. L. Quartapelle, Numerical solution of the incompressible Navier–Stokes equations (Birkhäuser, Berlin, 1993).
13. A. Thom, The flow past circular cylinders at low speeds, *Proc. Roy. Soc. London A* **141,** 651 (1933).
14. X. H. Wu, J. Z. Wu, and J. M. Wu, Effective vorticity-velocity formulations for three-dimensional incompressible viscous flows, *J. Comput. Phys.* **122,** 68 (1995).